Theoretical study of evaporation residue cross sections in the decay of ^{286}Cn* formed via the ^{238}U + ^{48}Ca reaction using Skyrme forces

Nirupama Kumari, Aman Deep, and Rajesh Kharab
Department of Physics, Kurukshetra University, Kurukshetra 136119, India

(Received 29 July 2021; accepted 11 January 2022; published 27 January 2022)

The dynamical cluster-decay model (DCM) is employed to study the excitation functions and fusion evaporation residue (ER) cross sections for the production of ^{283}Cn and ^{282}Cn isotopes via 3n and 4n decay channels from the ^{286}Cn* compound nucleus. The study includes quadrupole deformation β_{2i} and hot-optimum orientations θ_i at various ^{48}Ca-beam energies $E_{\rm lab}$ = 233.3–240 MeV (equivalently, excitation energies E^* = 34.4–39.8 MeV), supporting symmetric fission, which agrees well with the experimental data. The reaction was investigated by using a hot compact configuration. The Skyrme forces used are new forces GSkI and KDE0(v1), and the conventional force SIII. Apparently, the DCM with the pocket formula for nuclear proximity potential reproduces the measured data on fusion ER nicely within single-parameter fitting of ΔR, independently of the nuclear interaction potential and Skyrme force used. We have also calculated the fusion-fission cross section ($\sigma_{ff}^{\rm predicted}$) at E^* = 35 MeV and ER cross sections for the experimentally unobserved neutron emission channels 1n, 2n, and 4n at different excitation energies E^*. Further, we have proposed new target-projectile (t-p) combinations for the synthesis of ^{286}Cn for future experiments.

DOI: 10.1103/PhysRevC.105.014628

I. INTRODUCTION

The establishment of the center of an island of stability in the region of superheavy nuclei has been a long-standing problem of nuclear structure studies, i.e., to identify the next doubly magic nucleus (magic Z and magic N) heavier than ^{208}Pb [1]. The stability of superheavy nuclei depends strongly on shell effects and increases significantly at closed proton and neutron shells. For instance, beyond uranium the stability of these nuclei lessens quickly with the increasing element number Z and increases sharply when their neutron number approaches the spherical shell closure. According to various theoretical models, the next spherical shell closure for the neutrons beyond neutron number N = 126 is predicted at N = 184 [2–4]. Thus, to synthesize spherical superheavy nuclide, it is more appropriate to select reaction partners with the highest possible number of neutrons as close as possible to N = 184 in order to approach the shell closure [5]. During the last three decades transfermium elements with Z = 107–112 were synthesized through the so-called cold fusion reactions using lead and bismuth targets [6]. The advantage of these reactions is that only slightly excited (E^* = 10–20 MeV) compound nuclei are produced at bombarding energies near the fusion barrier. This is an outcome of the double magic structure of the ^{208}Pb target and the strongly bound projectiles from ^{54}Cr to ^{70}Zn. The main reason behind survival against prompt fission is considered to be the low excitation energies of fragile heavy compound nuclei. The isotopes of the elements Z = 102–112 were also synthesized through hot fusion reactions using targets Th to Cf [7,8]. However the excitation energies of compound nuclei are relatively high (30–50 MeV) in case of hot fusion reactions in comparison to cold fusion reactions, which results in reduction of the survival probability of compound nuclei in hot fusion reactions. It can be partially compensated by using highly asymmetric target-projectile (t-p) combinations [5] such as ^{238}U + ^{48}Ca leading to enhanced cross section for the formation of a compound nucleus. Therefore various asymmetric t-p combinations have been used to synthesize superheavy elements through hot fusion reactions [9]. Among these, the reactions induced by the doubly magic ^{48}Ca nucleus on the deformed reaction partner ^{238}U has attracted a lot of attention because, from the point of view of a cold reaction, the fusion barrier is lowest for the ^{48}Ca plus deformed-target combination as compared to other t-p combinations. Further, it provides suitable platform to investigate the role of deformation and orientation in the fusion reaction as studied in [9] using the proximity potential. Therefore the combination ^{238}U + ^{48}Ca has been used to produce isotopes of the superheavy element copernicium (Z = 112) through neutron evaporation from ^{286}Cn* [8,10–13] and is studied theoretically in the present work. It is worth mentioning here that the Cn is a d-block transactinide element and belongs to group 12 elements in the periodic table. Recently it was found that Cn is a relativistic noble liquid and also it is of medicinal importance in treatment of cancers and tumors by using Cn nanoparticles [14,15].

Theoretically various models/approaches like the dynamical cluster-decay model (DCM) [9,16], the Langevin model [17,18], time-dependent Hartree-Fock [19–21], and the dinuclear system (DNS) model [22,23] have been used to describe the dynamics of fusion-fission processes. However, in the present study the excitation function of ^{286}Cn* formed via

$^{238}U + ^{48}Ca$ reaction has been studied within the framework of the DCM using Skyrme forces. Theoretically the DCM, wherein the neck-lenth parameter ΔR is the only parameter, is based on the quantum mechanical fragmentation theory (QMFT) and is an excellent framework to describe the synthesis of superheavy elements. Here, we have used the DCM to analyze the excitation function of $^{286}Cn^*$ produced in the $^{238}U + ^{48}Ca$ reaction by using the nuclear potential derived from the Skyrme energy density formalism (SEDF) [24–26] based on the semiclassical extended Thomas-Fermi (ETF) approach under the frozen density approximation [27]. Specifically, the conventional SIII and newer GSkI and KDE0(v1) Skyrme forces have been used, and it has been found that all three chosen Skyrme forces fit the data nicely for $3n$-$4n$ decays from $^{286}Cn^*$, for which the measured ER cross sections are maximum. However, for the production of $^{286}Cn^*$, the experiments suggest that the hot compact configuration is preferred over the cold elongated configuration [8]. Nevertheless we have made our calculations for both the cold elongated and hot compact configurations.

Now, the questions we would like to answer are whether or not the excitation functions for both hot and cold processes depend on the nuclear interaction, and whether or not the production cross section depends on the mass asymmetry $[\eta = (A_2 - A_1)/(A_1 + A_2)]$ of the reaction system in the entrance channel. Also, we would like to identify, among all the possible t-p combinations that form a cold compound nucleus (CN), which one is most probable and results in largest cross section. Further, we would also like to predict the fission cross section for $^{286}Cn^*$.

In the following, we find that exactly the same t-p combinations as are used in the experiment [8,12], plus a few more, are suggested for the synthesis of CN $^{286}Cn^*$ on the basis of the Skyrme force included the DCM. Thus, the aim of this paper is at least fourfold: First, we search for the optimal reaction partners for the synthesis of the $^{286}Cn^*$ compound system other than those already used in experiments. Second, depending on the choice of orientation degree of freedom (cold or hot configuration), does the CN $^{286}Cn^*$ fission via symmetric or asymmetric mass distribution? Third, we analyze excitation functions data for $3n$ and $4n$ emission (ER cross sections σ_{xn}, $x = 3$–4, as a function of excitation energy E^*) in the decay of $^{286}Cn^*$ in terms of a single parameter of the model, the neck-length parameter ΔR. Finally we predict the fission cross section of $^{286}Cn^*$.

The paper is organized as follows. Section II gives the very relevant details of the theoretical model used, comprising the QMFT and the DCM, and of SEDF in the semiclassical approach. In Sec. III the formation of compound nucleus $^{286}Cn^*$ in terms of the QMFT and its decay via $3n$ and $4n$ emission by using the DCM are studied. The discussion of our results and a summary constitute Sec. IV.

II. THEORETICAL FORMALISM

In this section, we first introduce the well-known quantum mechanical fragmentation theory (QMFT) [28–33] and then describe the very essential details of the DCM based on QMFT and SEDF in the semiclassical ETF approach.

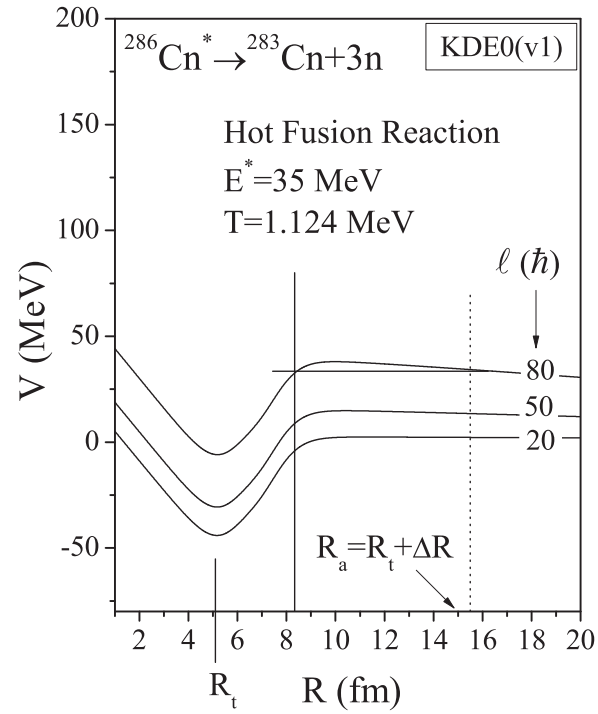

FIG. 1. Scattering potentials $V(R, \ell)$ for $^{286}Cn^* \rightarrow ^{283}Cn^* + 3n$ at excitation energy $E^* = 35$ MeV and at fixed temperature $T = 1.124$ MeV at different angular momentum ℓ values varying from $\ell_{min} = 20\hbar$ to $\ell_{max} = 80\hbar$ for the Skyrme force KDE0(v1) ($\ell < \ell_{min}$ do not contribute).

A. The dynamical cluster-decay model (DCM)

When a projectile having energy larger than the barrier energy is projected onto some target, compound nucleus formation takes place. If the so formed nuclear system is heavy enough, i.e., $A_{CN} \geqslant 200$, then the most probable decay mode is fragment emission. The process of decay through fragments can be described very well within the framework of the DCM based on QMFT.

The DCM [16,34–54] is worked out in terms of collective coordinates of mass [and charge] asymmetry $\eta = (A_1 - A_2)/(A_1 + A_2)$ [and $\eta_Z = (Z_1 - Z_2)/(Z_1 + Z_2)$], and relative separation R, the multipole deformations $\beta_{\lambda i}$, and orientations

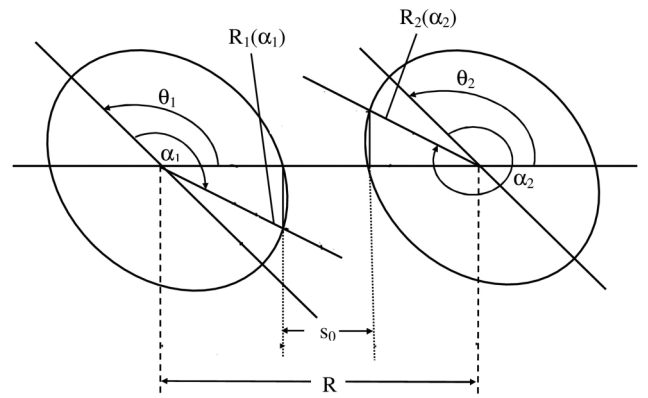

FIG. 2. Schematic diagram showing the angles (θ_1, θ_2, α_1, and α_2).

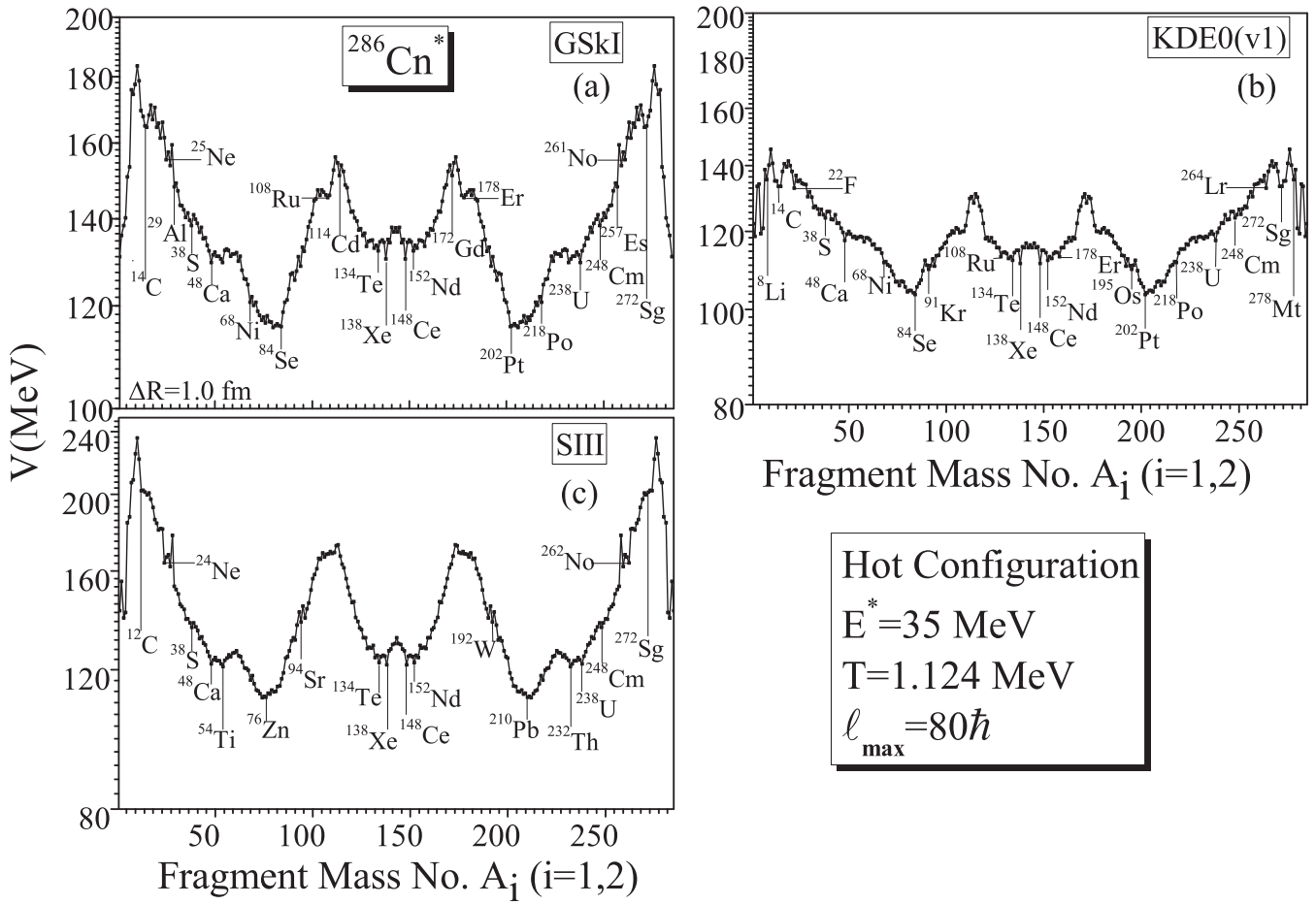

FIG. 3. Mass fragmentation potential $V(A_i)$, $i = 1, 2$ at $\ell = \ell_{\max}$ for the formation of CN ^{286}Cn* at $T = 1.124$ MeV corresponding to E^*=35 MeV, calculated at fixed $R = R_t + \Delta R$ with $\Delta R = 1.0$ fm, and with β_{2i} deformations and "optimum hot" orientations included for all possible t-p combinations, using Skyrme forces (a) GSkI, (b) KDE0(v1), and (c) SIII.

θ_i $(i = 1, 2)$ of two nuclei in the same plane. Here A_1 and A_2 (Z_1 and Z_1) are the mass (charge) numbers of fragments and $A_1 + A_2$ $(= A)$ is the mass number of the compound nucleus. In the DCM, using decoupled approximation to R and η motion, we define the compound nucleus decay (or fragment production) cross section in terms of partial wave analysis which is given as

$$\sigma = \sum_{\ell=0}^{\ell_{\max}} \sigma_\ell = \frac{\pi}{k^2} \sum_{\ell=0}^{\ell_{\max}} (2\ell + 1) P_0^\ell P_\ell, \quad k = \sqrt{\frac{2\mu E_{\text{c.m.}}}{\hbar^2}}, \quad (1)$$

where the preformation probability P_0^ℓ refers to η motion and the penetrability P_ℓ to R motion. $\ell_{\max}$ is the maximum angular momentum, fixed here for the light particle cross section approaching zero, i.e., $\sigma_{\text{ER}}(\ell) \to 0$ at $\ell = \ell_{\max}$, $\mu = [A_1 A_2/(A_1 + A_2)]m = \frac{1}{4} Am(1 - \eta^2)$ is the reduced mass with m the nucleon mass, and $E_{\text{c.m.}}$ is the entrance channel center-of-mass (c.m.) energy.

P_0 for each ℓ is the solution of the stationary Schrödinger equation in η, at fixed $R = R_a$, the first turning point(s) of the penetration path(s) (illustrated, e.g., in Fig. 1 for different ℓ values):

$$\left[-\frac{\hbar^2}{2\sqrt{B_{\eta\eta}}} \frac{\partial}{\partial \eta} \frac{1}{\sqrt{B_{\eta\eta}}} \frac{\partial}{\partial \eta} + V(\eta) \right] \psi^\nu(\eta) = E_\eta^\nu \psi^\nu(\eta), \quad (2)$$

with $\nu = 0, 1, 2, 3, \ldots$ referring to ground-state ($\nu = 0$) and excited-states solutions. Above, V is a potential which in general depends on various quantities like η, R, ℓ, T, β, θ, etc.; however, only η dependence is explicitly shown here for brevity. The mass parameters $B_{\eta\eta}$ in Eq. (2) are the smooth classical hydrodynamical masses [55], used for simplicity. In principle, the shell corrected masses, like the Cranking masses, should be used. The probability

$$P_0(A_i) = |\psi(\eta(A_i))|^2 \sqrt{B_{\eta\eta}} \frac{2}{A}, \quad (3)$$

where, for a Boltzmann-like function,

$$|\psi|^2 = \sum_{\nu=0}^{\infty} |\psi^\nu|^2 \exp(-E^\nu/T). \quad (4)$$

P_0 contains the structure information of the compound nucleus, which enter via the fragmentation potential.

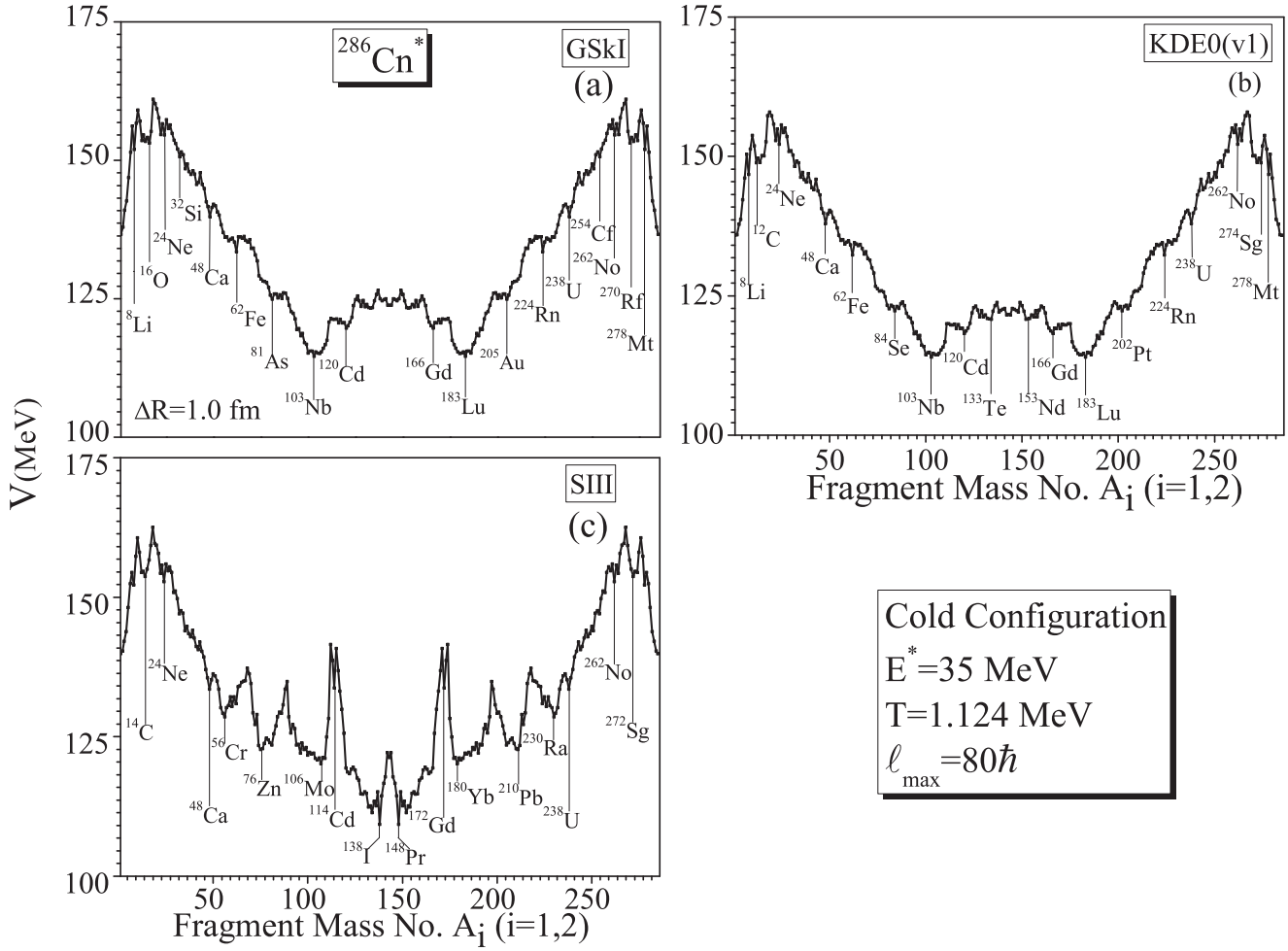

FIG. 4. Same as Fig. 3, but for "optimum cold" orientations.

The penetrability P_ℓ is the Wentzel-Kramers-Brillouin (WKB) integral between R_a and R_b,

$$P_\ell = \exp\left[-\frac{2}{\hbar}\int_{R_a}^{R_b}\{2\mu[V(R,\ell)-Q_{\rm eff}]\}^{1/2}dR\right], \quad (5)$$

with R_b as the second turning point, satisfying

$$V(R_a,\ell) = V(R_b,\ell) = Q_{\rm eff}(T,\ell) = {\rm TKE}(T). \quad (6)$$

Here TKE(T) is the temperature-dependent total kinetic energy. The ℓ dependence of R_a is defined by

$$V(R_a,\ell) = Q_{\rm eff}(T,\ell=\ell_{\rm min}), \quad (7)$$

which means that R_a, given by Eq. (7), is the same for all ℓ values, and that $V(R_a,\ell)$ acts like an effective Q value, $Q_{\rm eff}(T,\ell)$, given by the total kinetic energy TKE(T). $\ell_{\rm min}$ refers to the minimum value that starts to contribute to the WKB integral. Apparently, as the ℓ value increases, the $Q_{\rm eff}(T)$ value [= TKE(T)] increases and hence $V(R_a,\ell)$ increases (see Fig. 1).

For the decay of a hot compound nucleus, we use the following postulate for the first turning point:

$$\begin{aligned} R_a(T) &= R_1(\alpha_1,T) + R_2(\alpha_2,T) + \Delta R(T) \\ &= R_t(\alpha_1,\alpha_2,T) + \Delta R(T), \end{aligned} \quad (8)$$

with $\Delta R(T)$ as the neck-length parameter, assimilating the neck formation effects [56,57]. This method of introducing a neck-length parameter is similar to that used in both the scission-point [58] and saddle-point [59,60] statistical fission models. Note that $R_a(T)$ in Eq. (8) are α dependent since $R_t(T)$ are different for different α values.

Then, the deformation and orientation dependent fragmentation potential $V(\eta)$ in Eq. (2), at any temperature T, is given as

$$\begin{aligned} V(\eta,T) = &\sum_{i=1}^{2} V_{\rm LDM}(A_i,Z_i,T) + \sum_{i=1}^{2}\delta U\exp\left(-\frac{T^2}{T_0^2}\right) \\ &+ V_C(R,Z_i,\beta_{\lambda i},\theta_i,T) + V_\ell(R,A_i,\beta_{\lambda i},\theta_i,T) \\ &+ V_N(R,A_i,\beta_{\lambda i},\theta_i,T). \end{aligned} \quad (9)$$

Here, $V_{\rm LDM}$ is the T-dependent liquid drop energy of Davidson *et al.* [61] with its constants at $T=0$ refitted in Refs. [39,40,44,62]. The shell correction δU calculations are done with the help of the "empirical" estimates of Myers and Swiatecki [63]. The Coulomb potential for a multipole-multipole interaction between two separated, deformed, and

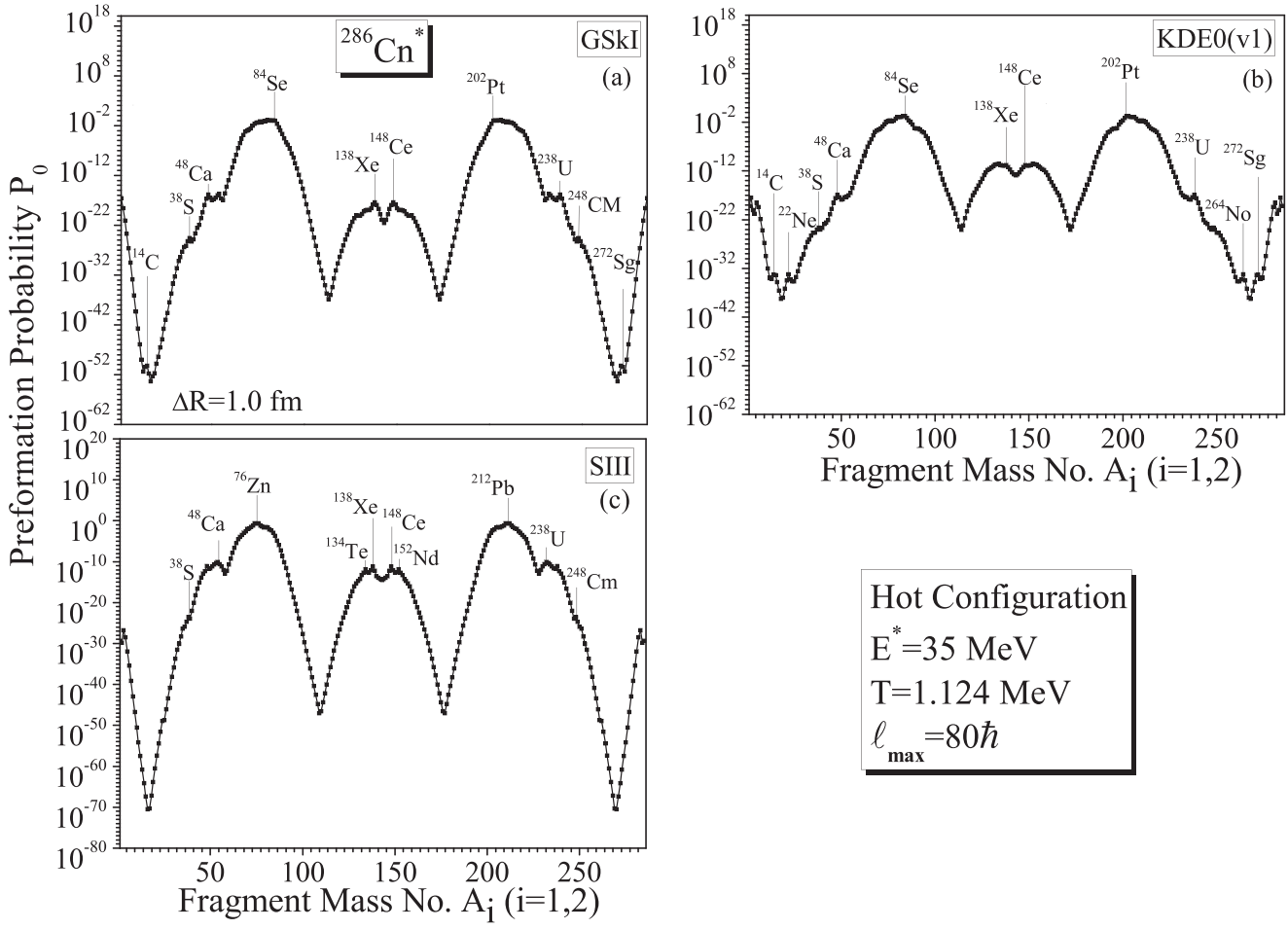

FIG. 5. Preformation yields for "hot configurations" referring to the fragmentation potentials in Fig. 3.

oriented nuclei is

$$V_C = \frac{Z_1 Z_2 e^2}{R} + 3Z_1 Z_2 e^2 \sum_{\lambda,i=1,2} \frac{R_i^\lambda(\alpha_i, T)}{(2\lambda+1)R^{\lambda+1}} \times Y_\lambda^{(0)}(\theta_i)\left[\beta_{\lambda i} + \frac{4}{7}\beta_{\lambda i}^2 Y_\lambda^{(0)}(\theta_i)\right], \quad (10)$$

with θ_i and α_i the angles as shown in Fig. 2, and the angular momentum dependent potential is

$$V_\ell = \frac{\hbar^2 \ell(\ell+1)}{2I} \quad (11)$$

with $I = I_S = \mu R^2 + \frac{2}{5}A_1 m R_1^2(\alpha_1, T) + \frac{2}{5}A_2 m R_2^2(\alpha_2, T)$, the moment of inertia in the sticking limit. V_N is the nuclear interaction potential discussed in the next subsection.

Apparently, in the DCM, both the light particles ($A_2 \leqslant 4$ or 5), referring to ER, and the complex, heavy mass fragments, referring to fusion-fission (ff) processes, are treated as the dynamical collective mass motion of preformed clusters or fragments through the barrier. The same formula [Eq. (1)] is also applicable to the noncompound, competing quasifission (qf) decay channel σ_{qf} where $P_0 = 1$ for the incoming channel, since both the target and projectile nuclei can be considered to have not yet lost their identity.

B. Nuclear interaction potential based on SEDF in the semiclassical ETF approach

The nuclear interaction potential within the energy density formalism is defined as (see, e.g., [64,65])

$$V_N(R) = E(R) - E(\infty), \quad (12)$$

i.e., the nucleus-nucleus interaction potential as a function of separation distance, $V_N(R)$, is the difference of the energy expectation value E of the colliding nuclei that are overlapping (at a finite separation distance R) and are completely separated (at $R = \infty$), where

$$E = \int H(\vec{r}) d\vec{r}, \quad (13)$$

For the Skyrme interaction the energy density $H(\vec{r})$ is an algebraic function of the nucleon densities ρ_n (ρ_p), the kinetic energy τ_n (τ_p) and spin densities $\vec{J}_n$ ($\vec{J}_p$). The Skyrme

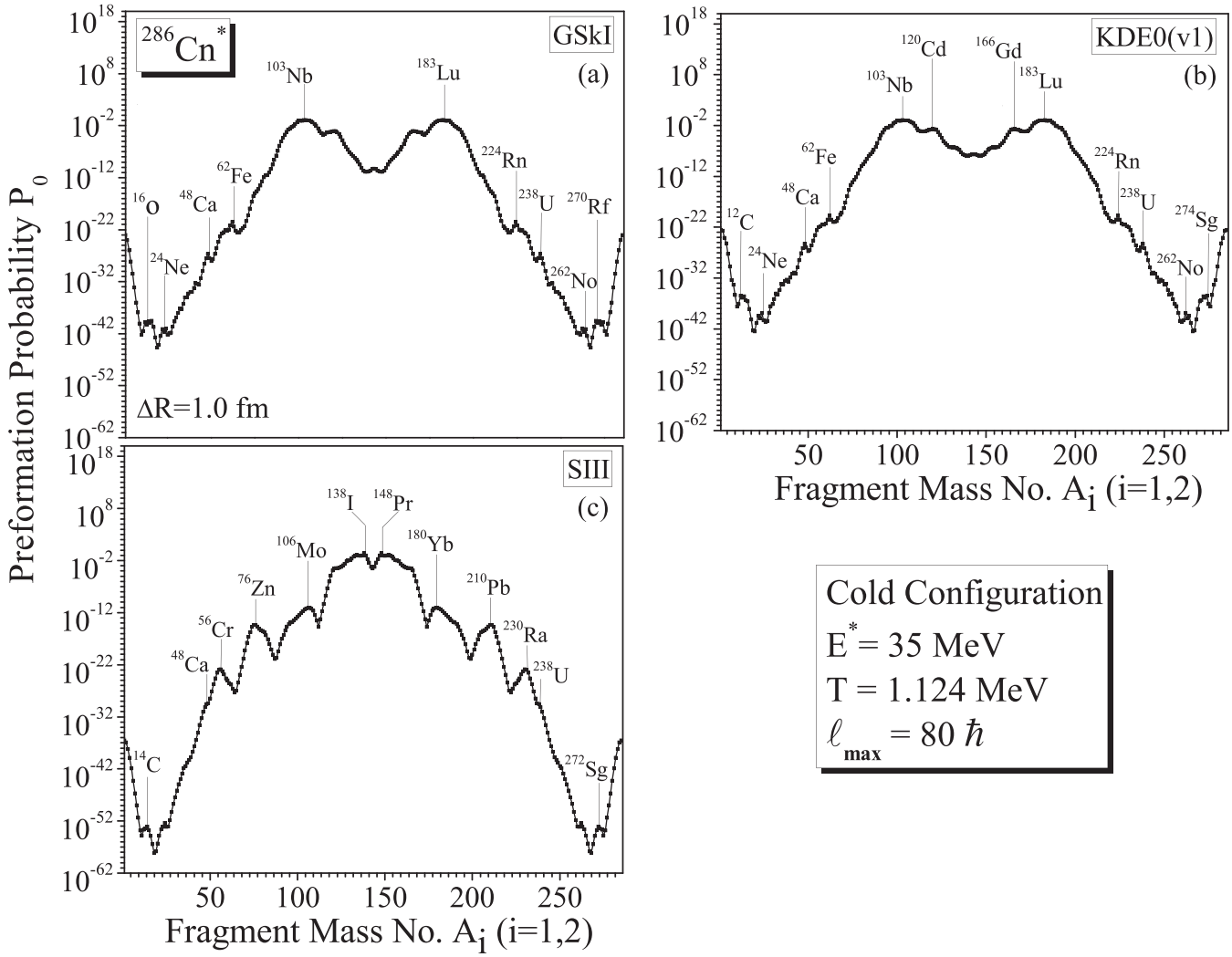

FIG. 6. Preformation yields for "cold configurations" referring to the fragmentation potentials in Fig. 4.

Hamiltonian density is defined as [66,67]

$$
\begin{aligned}
H(\rho,\tau,\vec{J}) = {} & \frac{\hbar^2}{2m}\tau + \frac{1}{2}t_0\left[\left(1+\frac{1}{2}x_0\right)\rho^2 - \left(x_0+\frac{1}{2}\right)\left(\rho_n^2+\rho_p^2\right)\right] + \frac{1}{2}\sum_{i=1}^{3} t_{3i}\rho^{\alpha_i}\left[\left(1+\frac{1}{2}x_{3i}\right)\rho^2 - \left(x_{3i}+\frac{1}{2}\right)\left(\rho_n^2+\rho_p^2\right)\right] \\
& + \frac{1}{4}\left[t_1\left(1+\frac{1}{2}x_1\right) + t_2\left(1+\frac{1}{2}x_2\right)\right]\rho\tau - \frac{1}{4}\left[t_1\left(x_1+\frac{1}{2}\right) - t_2\left(x_2+\frac{1}{2}\right)\right](\rho_n\tau_n+\rho_p\tau_p) \\
& + \frac{1}{16}\left[3t_1\left(1+\frac{1}{2}x_1\right) - t_2\left(1+\frac{1}{2}x_2\right)\right](\vec{\nabla}\rho)^2 - \frac{1}{16}\left[3t_1\left(x_1+\frac{1}{2}\right) + t_2\left(x_2+\frac{1}{2}\right)\right][(\vec{\nabla}\rho_n)^2 + (\vec{\nabla}\rho_p)^2] \\
& - \frac{1}{2}W_0[\rho\vec{\nabla}\cdot\vec{J} + \rho_n\vec{\nabla}\cdot\vec{J}_n + \rho_p\vec{\nabla}\cdot\vec{J}_p] - C\left[\frac{1}{16}(t_1x_1+t_2x_2)\vec{J}^2 - \frac{1}{16}(t_1-t_2)\left(\vec{J}_p^2+\vec{J}_n^2\right)\right].
\end{aligned} \tag{14}
$$

Here, $\rho = \rho_n + \rho_p$, $\tau = \tau_n + \tau_p$, and $\vec{J} = \vec{J}_n + \vec{J}_p$ are the nuclear, kinetic energy, and spin-orbit densities for the composite system, respectively. m is the nucleon mass, and x_j, t_j $(j = 0, 1, 2)$, x_{3i}, t_{3i}, α_i $(i = 1, 2, 3)$, W_0, and C are the Skyrme force parameters, fitted by different authors to ground state properties of various nuclei. For a conventional force [25], like SIII, some constants [C, x_{3i}, t_{3i}, and α_i $(i = 2, 3)$] are zero, and $t_{31} = \frac{1}{6}t_3$, $x_{31} = x_3$, and $\alpha_1 = \alpha$. Then, for newer forces of Agrawal *et al.* [66,68], like GSkI and KDE0(v1), we have $C = 1$ and six additional constants [two each of x_{3i}, t_{3i} and α_i], determined by a fit to several properties of the normal and isospin-rich nuclei.

TABLE I. The t-p combinations (A_1, A_2), referring to minima in the potential energy surface (PES) at $\ell_{max} = 80\hbar$ and for quadrupole deformed and "optimum cold" oriented nuclei forming the CN ^{286}Cn* at $T = 1.124$ MeV ($E^* = 35$ MeV) for the illustrative KDE0(v1) Skyrme force, and their other characteristic properties.

Reaction $A_1 + A_2$	β_{21}	β_{22}	V_B (MeV)	R_B (fm)
^{278}Mt + ^{8}Li	0.136	−0.09	76.645	9.79
^{272}Sg + ^{14}C	0.201	−0.016	108.179	10.34
^{264}Lr + ^{22}F	0.22	−0.028	138.825	10.96
^{248}Cm + ^{38}S	0.235	0.0	182.966	12.06
^{238}U + ^{48}Ca	0.215	0.0	207.605	12.47
^{218}Po + ^{68}Ni	0.039	0.018	249.316	13.08
^{202}Pt + ^{84}Se	−0.061	0.053	281.344	12.92
^{195}Os + ^{91}Kr	0.127	0.209	293.468	12.72
^{178}Er + ^{108}Ru	0.279	0.283	329.629	12.25
^{152}Nd + ^{134}Te	0.262	0.0	338.994	12.51
^{148}Ce + ^{138}Xe	0.216	0.0	339.095	12.97

The kinetic energy density in the ETF method, considered here up to second-order terms for reasons of being enough for numerical convergence [26], is ($q = n$ or p)

$$\tau_q(\vec{r}) = \frac{3}{5}(3\pi^2)^{2/3}\rho_q^{5/3} + \frac{1}{36}\frac{(\vec{\nabla}\rho_q)^2}{\rho_q} + \frac{1}{3}\Delta\rho_q + \frac{1}{6}\frac{\vec{\nabla}\rho_q\cdot\vec{\nabla}f_q + \rho_q\Delta f_q}{f_q} - \frac{1}{12}\rho_q\left(\frac{\vec{\nabla}f_q}{f_q}\right)^2 + \frac{1}{2}\rho_q\left(\frac{2m}{\hbar^2}\right)^2\left(\frac{W_0}{2}\frac{\vec{\nabla}(\rho+\rho_q)}{f_q}\right)^2, \quad (15)$$

with f_q as the effective mass form factor,

$$f_q(\vec{r}) = 1 + \frac{2m}{\hbar^2}\frac{1}{4}\left\{t_1\left(1+\frac{x_1}{2}\right) + t_2\left(1+\frac{x_2}{2}\right)\right\}\rho(\vec{r}) - \frac{2m}{\hbar^2}\frac{1}{4}\left\{t_1\left(x_1+\frac{1}{2}\right) - t_2\left(x_2+\frac{1}{2}\right)\right\}\rho_q(\vec{r}). \quad (16)$$

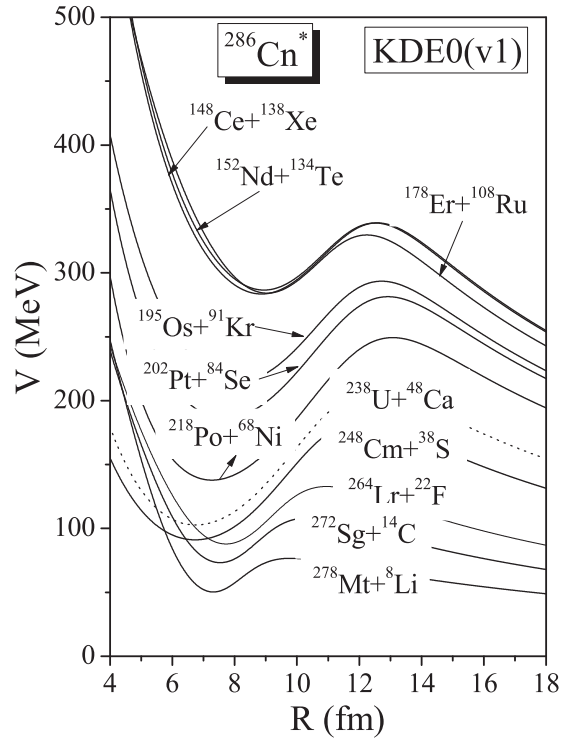

FIG. 7. Scattering potentials $V(R)$ for "hot fusion" reaction valleys with "hot-compact" configurations of Fig. 3(b) at a fixed temperature $T = 1.124$ MeV (E^*=35 MeV) and $\ell_{max} = 80\hbar$, illustrated for KDE0(v1) Skyrme force. The potentials for the t-p combinations predicted for future experiments are shown by solid lines while for that used in experiments [8,12] is shown by a dotted line.

Note that both τ_q and f_q are each a function of ρ_q and/or ρ only.

The spin-orbit density $\vec{J}$ is a purely quantal property, and hence has no contribution in the lowest Thomas-Fermi (TF) order. However, at the ETF level, the second-order contribution gives

$$\vec{J}_q(\vec{r}) = -\frac{2m}{\hbar^2}\frac{1}{2}W_0\frac{1}{f_q}\rho_q\vec{\nabla}(\rho+\rho_q), \quad (17)$$

also a function of ρ_q and/or ρ alone.

TABLE II. The excitation function of 3n and 4n evaporation channels from ^{286}Cn* due to entrance channel ^{238}U + ^{48}Ca calculated by using the DCM for a best fit of ΔR, at different $E^* = 34.4$ to 39.8 MeV energies for various Skyrme forces, compared with experimental data [8,12], and also with results from Wu's calculation by DNS model [76] are shown in this table. The predicted fission cross section ($\sigma_{ff}^{predicted}$) for CN ^{286}Cn at $E^* = 35$ MeV is 1.63×10^{-12} mb for GSkI, 9.87×10^{-10} mb for KDE0(v1), and 3.38×10^{-17} mb for SIII Skyrme forces.

			DCM							
E^*		T	ΔR (fm)			$\sigma_{Calc.}^{DCM}$ (pb)				
(MeV)	xn	(MeV)	GSkI	KDE0(v1)	SIII	GSkI	KDE0(v1)	SIII	$\sigma_{Calc.}^{DNS}$ (pb)	$\sigma_{Expt.}$ (pb)
34.4	3n	1.114	1.7556	1.5558	1.9811	1.0	1.0	1.0		$1.0^{+1.0}_{-0.6}$
34.6	3n	1.118	1.7561	1.6120	1.9739	0.72	0.72	0.72		$0.719^{+0.58}_{-0.35}$
34.8	3n	1.121	1.7289	1.5365	1.9501	0.7	0.699	0.699		$0.701^{+1.6}_{-0.6}$
35	3n	1.124	1.7705	1.7396	1.9311	2.5	2.5	2.43	1.18	$2.5^{+1.8}_{-1.1}$
35	4n	1.124	2.1190	1.9350	2.2467	0.809	0.836	0.822		≈0.82
39.8	4n	1.197	2.0260	1.6411	2.1114	0.593	0.530	0.584	2.38	$0.6^{+1.6}_{-0.5}$

TABLE III. The excitation function of $1n$, $2n$, and $4n$ evaporation channels from ^{286}Cn* due to entrance channel ^{238}U + ^{48}Ca predicted by using the DCM for a best fit of ΔR, at different $E^* = 34.4$ to 39.8 MeV energies by using GSkI Skyrme forces.

E^* (MeV)	xn	T (MeV)	$\sigma^{\rm DCM}_{\rm predicted}$ (pb)
34.4	$1n$	1.114	8.86×10^{-11}
34.4	$2n$	1.114	6.30×10^{-13}
34.4	$4n$	1.114	3.49×10^{-17}
34.6	$1n$	1.118	6.0×10^{-11}
34.6	$2n$	1.118	4.23×10^{-13}
34.6	$4n$	1.118	2.31×10^{-17}
34.8	$1n$	1.121	1.53×10^{-10}
34.8	$2n$	1.121	1.12×10^{-12}
34.8	$4n$	1.121	6.68×10^{-17}
35	$1n$	1.124	1.57×10^{-10}
35	$2n$	1.124	1.11×10^{-12}
39.8	$1n$	1.197	7.34×10^{-10}
39.8	$2n$	1.197	3.97×10^{-12}
39.8	$3n$	1.197	3.16×10^{-13}

The densities for the composite system, under the frozen density approximation used here, are [27]

$$\begin{aligned} \rho &= \rho_1 + \rho_2, \\ \tau(\rho) &= \tau_1(\rho_1) + \tau_2(\rho_2), \\ \vec{J}(\rho) &= \vec{J}_1(\rho_1) + \vec{J}_2(\rho_2), \end{aligned} \tag{18}$$

with

$$\rho_i = \rho_{\rm in} + \rho_{ip}, \quad \tau_i(\rho_i) = \tau_{in}(\rho_{in}) + \tau_{ip}(\rho_{\rm ip}), \quad \text{and}$$
$$\vec{J}_i(\rho_i) = \vec{J}_{in}(\rho_{\rm in}) + \vec{J}_{ip}(\rho_{\rm ip}).$$

Then, following Blocki *et al.* [69] and Gupta *et al.* [70], for the nuclear proximity potential [41,71,72], we introduce the slab approximation with interaction energy per unit area $e(s)$ between two flat slabs of semi-infinite nuclear matter with surfaces parallel to the X-Y plane and moving in the z direction, and separated by distance s having minimum value s_0. Then, the interaction potential $V_N(R)$ between two nuclei

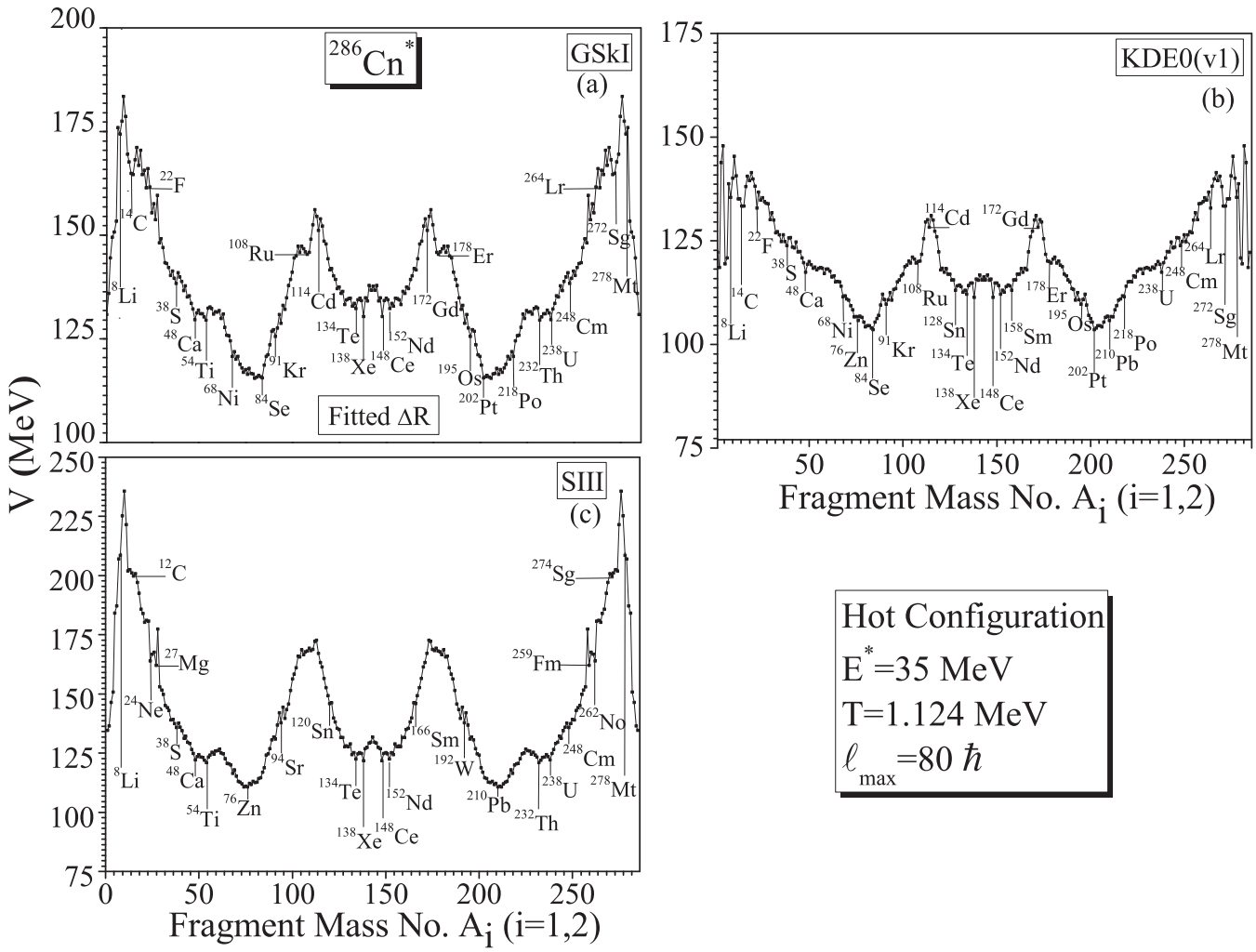

FIG. 8. Same as Fig. 3, but for $\Delta R_{3n,4n} = 1.7705$ and 2.1190 fm for GSkI force, $\Delta R_{3n,4n} = 1.7396$ and 1.9350 fm for KDE0(v1) force, and $\Delta R_{3n,4n} = 1.9311$ and 2.2467 fm for SIII force, which fit the data in Fig. 11 at $E^* = 35$ MeV for $3n$ and $4n$ emission from ^{286}Cn* formed via ^{238}U + ^{48}Ca reaction. The $\Delta R = 0.1$ fm is fixed for the light fragment masses $A_2 = 1$–2 and 5–143 (the complementary heavy fragments).

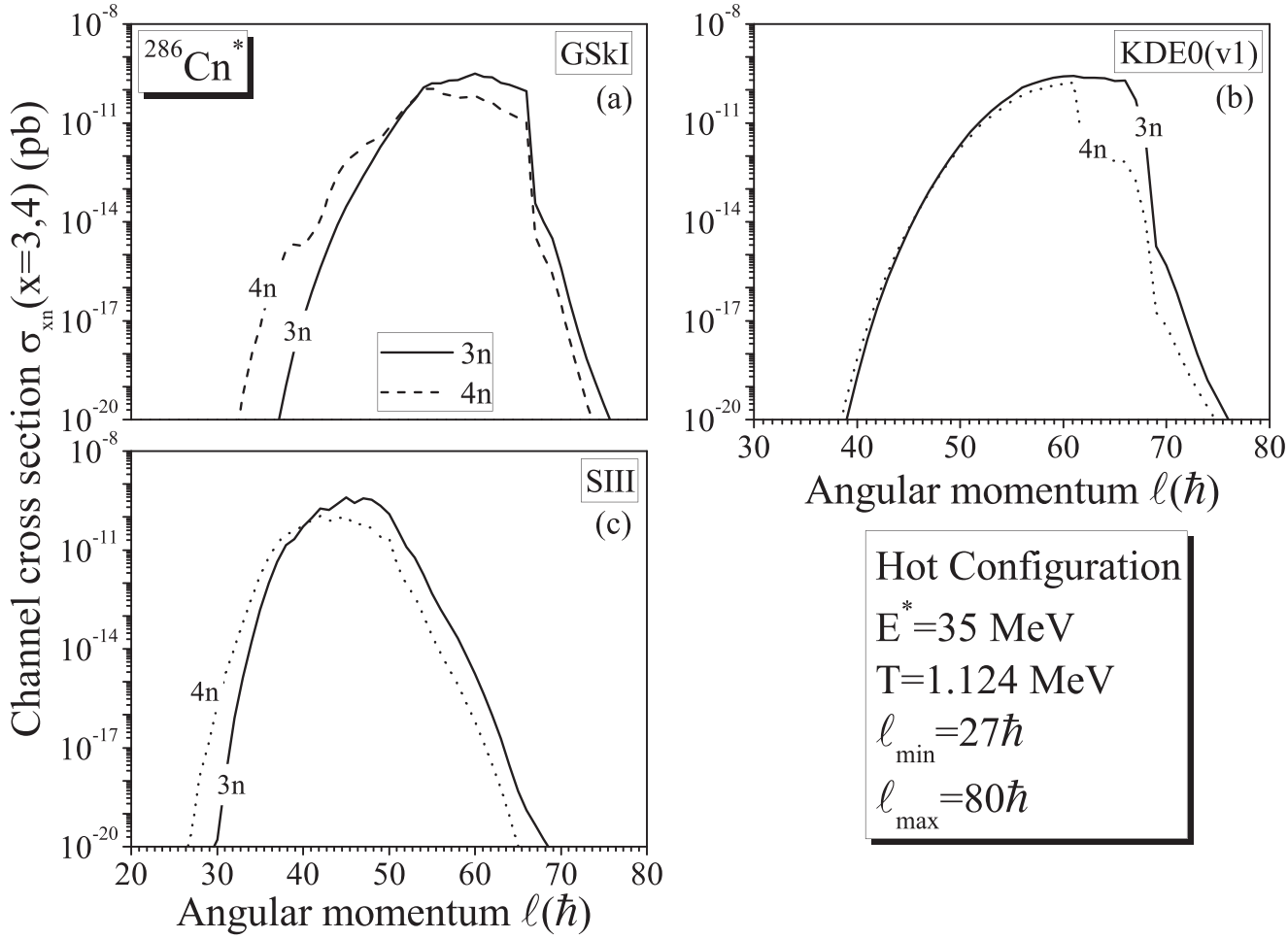

FIG. 9. Channel cross sections σ_{xn}, $x = 3$ and 4, for ^{286}Cn*, plotted as a function of ℓ; the cutoff point is $\sigma_{xn} < 10^{-20}$ pb, limiting $\ell_{\min} = 27\hbar$, $\ell_{\max} = 80\hbar$ for all three Skyrme forces.

separated by $R = R_1 + R_2 + s$, is given as

$$\begin{aligned} V_N(R) &= 2\pi\bar{R}\int_{s_0}^{\infty} e(s)ds \\ &= 2\pi\bar{R}\int \{H(\rho,\tau,\vec{J}) \\ &\quad -[H_1(\rho_1,\tau_1,\vec{J}_1)+H_2(\rho_2,\tau_2,\vec{J}_2)]\}dZ \\ &= 4\pi\bar{R}\gamma b\phi(D) = V_P(R)+V_J(R), \end{aligned} \tag{19}$$

where $V_P(R)$ and $V_J(R)$ are the spin-density independent and spin-density dependent parts of the nuclear interaction potential. H, H_1, and H_2 are the Hamiltonians of composite system and the separated nuclei respectively. $\bar{R} = R_1R_2/(R_1+R_2)$ is the mean curvature radius, defining the geometry of the system, and $\phi(D)$ is the universal function in terms of a dimensionless variable $D = s_0/b$, with b as the surface width. The nuclear surface energy constant $\gamma = 0.9517[1 - 1.7826(\frac{N-Z}{A})^2]$ MeV fm^{-2}. For further details on $\phi(D)$, etc., see Ref. [41].

For nuclear density ρ_i of each nucleus, the T-dependent, two-parameter Fermi density (FD) distribution for the slab approximation is given by [41]

$$\rho_i(z_i,\alpha_i,T) = \rho_{0i}(T)\left[1+\exp\left(\frac{z_i - R_i(T)}{a_i(T)}\right)\right]^{-1} \quad -\infty \leqslant z \leqslant \infty \tag{20}$$

with $z_2 = R - z_1 = [R_1(\alpha_1,T) + R_2(\alpha_2,T) + s] - z_1$ Here

$$\rho_{0i}(T) = \frac{3A_i}{4\pi R_i^3(T)}\left[1+\frac{\pi^2 a_i^2(T)}{R_i^2(T)}\right]^{-1}, \tag{21}$$

and

$$R_i(\alpha_i,T) = R_{0i}(T)\left[1+\sum_{\lambda}\beta_{\lambda i}Y_{\lambda}^{(0)}(\alpha_i)\right], \tag{22}$$

are the central density and the radii for deformed nuclei $R_i(\alpha_i,T)$ respectively. Above the T-dependent spherical or half-density nuclear radius R_{0i} and surface thickness parameters a_i are given by $R_{0i}(T) = R_{0i}(T=0)[1+0.0005T^2$ and $a_i(T) = a_i(T=0)[1+0.01T^2]$ and at $T = 0$ are obtained by fitting the experimental data [73,74] to respective polynomials

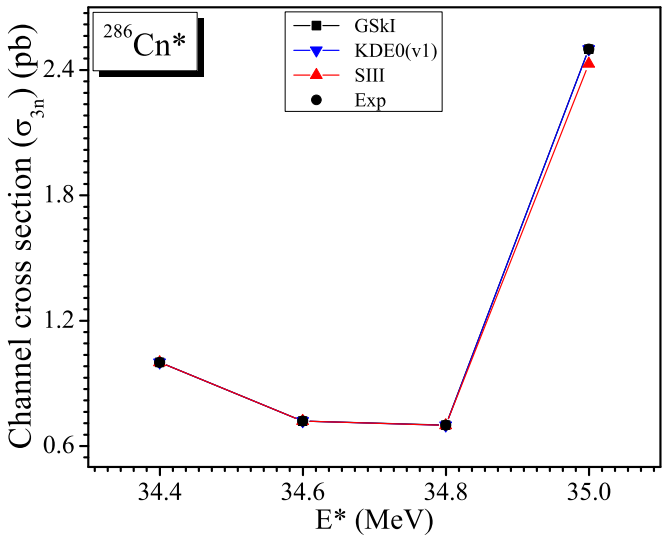

FIG. 10. Excitation function of individual $3n$ evaporation channels for the $^{238}\mathrm{U}+^{48}\mathrm{Ca}$ reaction in the "hot fusion" process. The experimental data (circle symbol) are from Ref. [8,12], and the rectangle, down triangle, and up triangle represent our calculations made for different Skyrme forces (a) GSkI, (b) KDE0(v1), and (c) SIII for the best fitted ΔR values given in Fig. 11. The calculations are made for the observed excitation energies E^*, and the lines or curves are to guide the eyes.

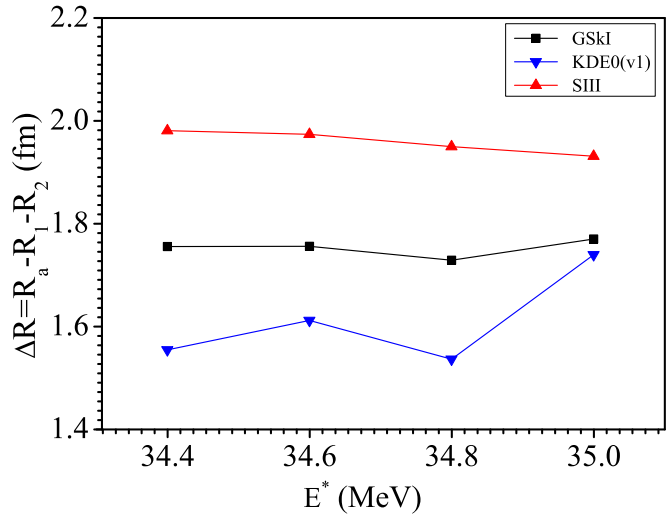

FIG. 11. The best fitted neck-length parameter ΔR as a function of E^* energy for $3n$ ER from $^{286}\mathrm{Cn}^*$ formed in reaction channel $^{238}\mathrm{U}+^{48}\mathrm{Ca}$ at excitation energy of 34.4–35 MeV. The rectangle, down triangle, and up triangle represent our calculations made for different Skyrme forces (a) GSkI, (b) KDE0(v1), and (c) SIII respectively.

in nuclear mass region $A = 4$–238 [41], as

$$\begin{aligned} R_{0i}(T=0) &= 0.9543 + 0.0994A_i - 9.8851\times10^{-4}A_i^2 \\ &\quad +4.8399\times10^{-6}A_i^3 - 8.4366\times10^{-9}A_i^4, \\ a_i(T=0) &= 0.3719 + 0.0086A_i - 1.1898\times10^{-4}A_i^2 \\ &\quad +6.1678\times10^{-7}A_i^3 - 1.0721\times10^{-9}A_i^4. \end{aligned} \quad (23)$$

In Eq. (22), $\lambda = 2, 3, 4, \ldots$ are the multipole deformations, and α_i are the angles between radius vector $R_i(\alpha_i)$ and the symmetry axis measured clockwise from the symmetry axis.

The temperature T is related to the incoming center-of-mass energy $E_{\mathrm{c.m.}}$ or the compound nucleus excitation energy E^* via the entrance channel Q_{in} value, as

$$E^* = E_{\mathrm{c.m.}} + Q_{in} = \frac{1}{a_c}AT^2 - T \quad (T \text{ in MeV}), \quad (24)$$

with a_c (a constant) $= 9$ or 10, respectively, for intermediate mass or superheavy systems. $Q_{in} = B_1 + B_2 - B_{\mathrm{CN}}$, with binding energies B's taken from [75]. Furthermore, since $\rho_i = \rho_{n_i} + \rho_{p_i}$, for nucleon density we define

$$\rho_{n_i} = (N_i/A_i)\rho_i \quad \text{and} \quad \rho_{p_i} = (Z_i/A_i)\rho_i. \quad (25)$$

III. CALCULATIONS AND DISCUSSION

In this section, we first identify all the possible t-p combinations (minima in potential energy surface, PES) at hot or cold orientations, i.e., hot-compact or cold-elongated configurations leading to the formation of CN $^{286}\mathrm{Cn}^*$ at a fixed temperature T and, among these, the most optimum reaction the giving largest fusion cross section. The best choice of either hot or cold configuration depends on the calculated yields compared with measured fission mass distribution. Then, in the next subsection, the decay of $^{286}\mathrm{Cn}^*$ for $3n$ and $4n$ emission is discussed. We have performed calculations using the DCM, with the nuclear interaction potential obtained from the SEDF-based ETF method for three illustrative Skyrme forces: GSkI, KDE0(v1), and SIII.

A. Synthesis of compound nucleus ^{286}Cn*

First, for the given compound nucleus $^{286}\mathrm{Cn}^*$, we calculate the fragmentation potential $V(\eta)$ for all possible t-p combinations (η values) forming optimum hot fusion configurations (or cold fusion configurations) at a fixed $\Delta R = 1.0$ fm for each Skyrme force. This is shown in Fig. 3 for hot and in Fig. 4 for cold configurations, using (a) GSkI (b) KDE0(v1), and (c) SIII forces. We notice from each of these two figures that all minima are nearly common for all the three forces i.e., all the three forces behave nearly alike since almost the same t-p combination refer to the minimum. Interestingly, in Fig. 3 for hot-fusion configurations, for all three cases, the potential energy minima occur at the symmetric fragmentation, whereas the same in Fig. 4 for cold-fusion configurations occur at the asymmetric fragmentation. The above results from fragmentation potentials can be better understood in terms of the corresponding production yields for the two cases (hot and cold fusion processes), shown in Figs. 5 and 6, respectively, for the fragmentation potentials in Figs. 3 and 4. We notice that, independently of the Skyrme force used, there is a strong dissimilarity in the hot and cold paths of fragmentation, and the symmetric fission mass distribution is given only for the hot fusion case, in complete

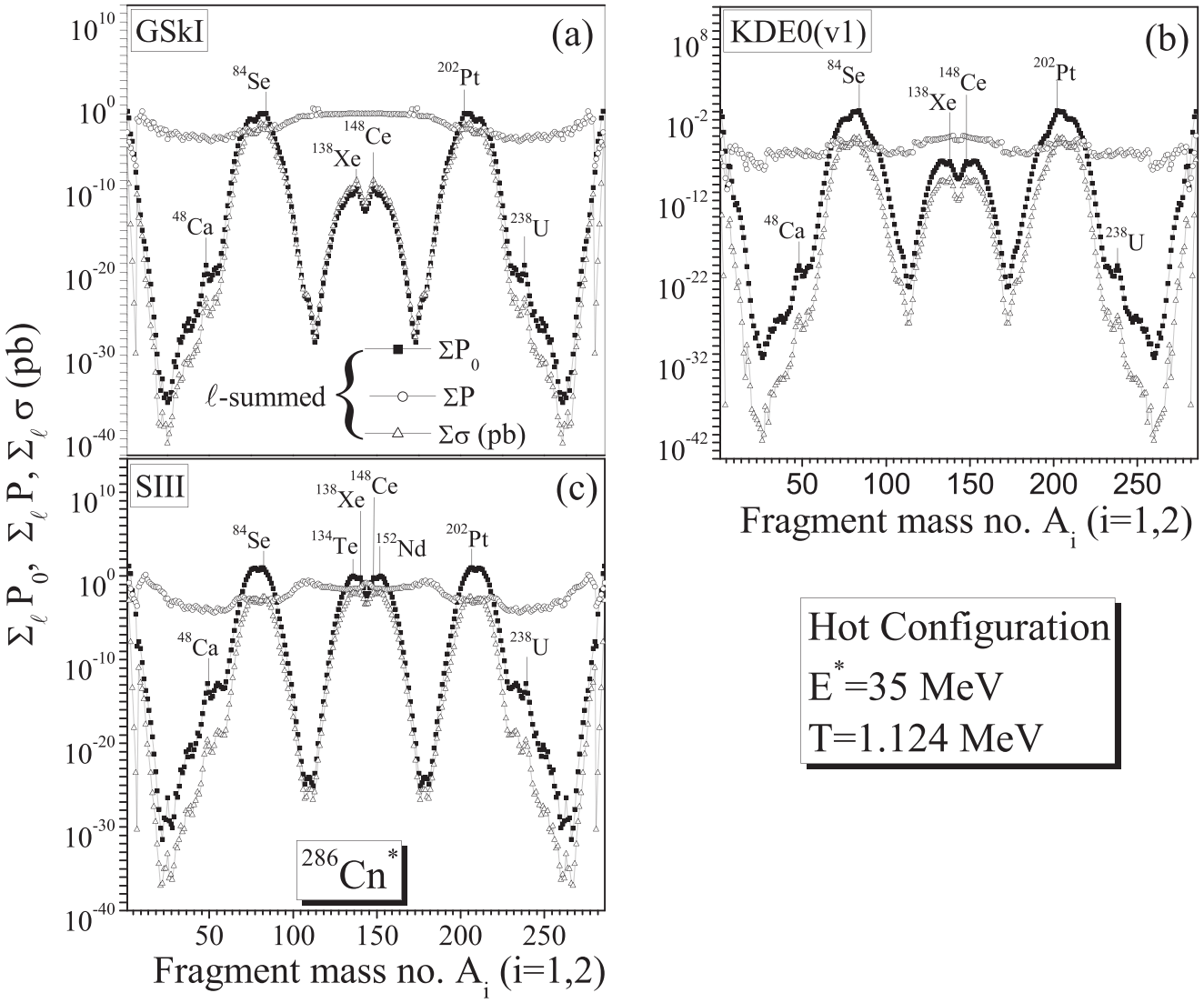

FIG. 12. ℓ-summed preformation probability P_0, penetration probability P, and channel cross section σ_{A_i}, $i = 1, 2$, plotted as a function of fragment mass number A_i.

accordance with experiments [8,12]. Hence, in the following, we focus only on hot fusion configurations, i.e., Figs. 3 and 5. The resulting t-p combinations, referring to minima in PES for the hot-fusion configuration, marked in Fig. 3, are listed in Table I for Skyrme force KDE0(v1), together with their other characteristics, i.e., quadrupole deformations β_{2i} [75], and calculated barrier heights V_B and positions R_B for optimum hot-compact orientations. We notice that, in addition to the ^{48}Ca-induced reaction, there are a few other possibilities; specifically, ^{278}Mt + ^{8}Li, ^{272}Sg + ^{14}C, ^{264}Lr + ^{22}F, ^{248}Cm + ^{38}S, ^{218}Po + ^{68}Ni, ^{202}Pt + ^{84}Se, ^{195}Os + ^{91}Kr, ^{178}Er + ^{108}Ru, ^{152}Pb + ^{134}Te, and ^{148}Ce + ^{138}Xe are suggested, in principle, for future experiments. However, because of the technical constraints on the preparation of targets, the best suited t-p combinations suggested here are ^{218}Po + ^{68}Ni and ^{202}Pt + ^{84}Se. Except for these reactions, many other reactions do not survive in the calculated yields due to the reduced shell effect at the considered temperature and low binding energies of incoming reaction partners, so other t-p combinations are not predictable. Hence, a theoretical basis for the choice of t-p combinations for the synthesis of ^{286}Cn*—which have so far been chosen by experimentalists simply on the basis of availability—is provided by QMFT. The next important task is to make an optimum choice of t-p combination for the production of CN ^{286}Cn with largest cross section. Note that all t-p combinations considered above refer to cold reaction valleys (minima in PES) with hot-compact configurations, which when put together means that the interaction radius is smallest and the interaction barrier is lowest [41,42]. Thus, of all the cold t-p combinations forming the same hot CN system, the optimum t-p refers to one with lowest interaction barrier and smallest (most compact) interaction radius. Figure 7 shows the interaction (scattering) potentials for all the t-p combinations given in Table I, which appear as minima in Fig. 3(b), together with the one ^{238}U + ^{48}Ca, which is used in experiment.

B. Decay of compound nucleus ^{286}Cn*

In this subsection, we estimate the light-particle decay channel cross sections σ_{xn}, the fusion-fission cross section $\sigma_{ff}^{\text{predicted}}$, and noncompound nucleus quasifission cross sections σ_{qf} using the DCM, for a best fit of ΔR to the measured data on decay of ^{286}Cn*, which is available only for σ_{xn}, $x = 3$ and 4. The fitting is done here for the reaction $^{238}\text{U} + ^{48}\text{Ca}$ for $E_{\text{lab}} = 233.3$–240 MeV using all the three chosen Skyrme forces. We have presented our calculated results in Table II and compared with experimental data [8,12], and also with results from Wu's calculation by the DNS model [76]. Further we have also calculated unobserved (experimentally) $1n$, $2n$, and $4n$ evaporation cross sections at different $E^* = 34.4$ to 39.8 MeV by using the DCM model with the application of GSkI Skyrme force, and corresponding results are shown in Table III.

For all three Skyrme forces used, Fig. 8 presents the calculated mass fragmentation potential $V(A_i)$, $i = 1, 2$ for the decay of CN ^{286}Cn* at maximum angular momentum ($l_{\max} = 80\hbar$, which is fixed later in Fig. 9), using the best fitted ΔR values (given in the figure caption) at $T = 1.124$ MeV corresponding to the incident energy $E_{\text{lab}} = 234$ MeV of the reaction $^{238}\text{U} + ^{48}\text{Ca}$. We note here that this fragmentation potential differs from the one in Fig. 3 since different decay products (here xn) occur in different timescales (different ΔR's) whereas the compound nucleus is formed at a fixed relative separation ΔR (fixed ΔR). Also, we observe that all three forces GSkI, KDE0(v1), and SIII behave nearly alike, except for the relative depths of their minima. Figure 9 presents the calculated channel cross section as a function of angular momentum for the reaction $^{238}\text{U} + ^{48}\text{Ca}$ and shows an increase with ℓ up to about $45\hbar$ for SIII, $60\hbar$ for GSkI, and $63\hbar$ for KDE0(v1) forces, but then a decrease with the increase of ℓ. Here we have fixed the maximum ($\ell_{\max}$) and minimum ($\ell_{\min}$) values of angular momentum for the calculated channel cross sections σ_{xn} for $x = 3$–4, which become negligibly small ($\sigma_{xn} < 10^{-20}$, $x = 3, 4$) for ℓ values other than those lying in the range $\ell_{\min} \leqslant \ell \leqslant \ell_{\max}$. Thus, for the limiting value of $\sigma_{xn} < 10^{-20}$, the window is set as $27\hbar \leqslant \ell \leqslant 80\hbar$, i.e., $\ell_{\max} = 80\hbar$ and $\ell_{\min} = 27\hbar$.

In Fig. 10, we have compared experimental and the DCM calculated σ_{xn}, $x = 3n$, from ^{286}Cn* at a fixed $E^* = 35$ MeV for the entrance channel $^{238}\text{U} + ^{48}\text{Ca}$. The experimental data are taken from Refs. [8,12] and the calculations are made for the neck-length parameter ΔR obtained for the best fit to $3n$ ER cross section from ^{286}Cn using the three Skyrme forces, namely (a) GSkI, (b) KDE0(v1), and (c) SIII, as plotted in Fig. 11. Here at each excitation energy E^*, the ΔR is largest for $4n$ emission followed by $3n$ emission (see Table II) from the compound system ^{286}Cn*, which suggests that the $4n$ emission occur earliest, then $3n$ emission, in complete agreement with experimental data implying that compound system ^{283}Cn* has the highest cross section and ^{282}Cn* the lowest. Clearly, as shown in Table II, for all the three forces, the $3n$ decay channel has the largest cross section, followed by $4n$ decay cross sections, in complete agreement with experimental results. Apparently, the DCM reproduces the data nicely within one-parameter fitting ΔR, nearly independent of the Skyrme force used.

TABLE IV. The DCM predicted ER cross sections σ_{xn} for $3n$ and $4n$ decay channels of ^{286}Cn*, formed in the "hot fusion" reaction proposed on the basis of QMFT, at $E^* = 35$ MeV, for all three Skyrme forces.

$A_1 + A_2$	σ_{3n}	σ_{4n}
	For Skyrme force GSkI	
$^{278}\text{Mt} + ^{8}\text{Li}$	6.28×10^{1}	3.96×10^{-2}
$^{272}\text{Sg} + ^{14}\text{C}$	3.03×10^{2}	6.12×10^{-1}
$^{264}\text{Lr} + ^{22}\text{F}$	3.26×10^{3}	2.36×10^{1}
$^{248}\text{Cm} + ^{38}\text{S}$	4.08×10^{5}	3.22×10^{-10}
$^{232}\text{Th} + ^{54}\text{Ti}$	4.29×10^{4}	2.33×10^{-7}
$^{202}\text{Pt} + ^{84}\text{Se}$	1.19×10^{-3}	7.43×10^{-8}
	For Skyrme force KDE0(v1)	
$^{278}\text{Mt} + ^{8}\text{Li}$	1.14×10^{0}	1.25×10^{-3}
$^{272}\text{Sg} + ^{14}\text{C}$	4.48×10^{-4}	6.87×10^{-7}
$^{264}\text{Lr} + ^{22}\text{F}$	2.07×10^{-1}	2.89×10^{-4}
$^{248}\text{Cm} + ^{38}\text{S}$	1.42×10^{-7}	1.55×10^{-12}
$^{232}\text{Th} + ^{54}\text{Ti}$	1.19×10^{-15}	4.05×10^{-26}
$^{202}\text{Pt} + ^{84}\text{Se}$	6.44×10^{-10}	2.37×10^{-16}
	For Skyrme force SIII	
$^{278}\text{Mt} + ^{8}\text{Li}$	8.95×10^{1}	1.82×10^{1}
$^{272}\text{Sg} + ^{14}\text{C}$	2.25×10^{1}	1.13×10^{-2}
$^{264}\text{Lr} + ^{22}\text{F}$	2.64×10^{0}	6.44×10^{-4}
$^{248}\text{Cm} + ^{38}\text{S}$	1.14×10^{-7}	7.87×10^{1}
$^{232}\text{Th} + ^{54}\text{Ti}$	1.65×10^{-16}	2.54×10^{-23}
$^{202}\text{Pt} + ^{84}\text{Se}$	1.91×10^{-10}	1.17×10^{-1}

Figure 12 shows a plot of ℓ-summed penetration probability P, preformation probability P_0, and channel cross-section σ_{xn}, plotted as a function of fragment mass number. We notice that, for all the three Skyrme forces, $P(A_i)$ is nearly constant and contributes only to the magnitude of cross section; $P_0(A_i)$ provides the structure to the cross section. An interesting result of this graph is that CN ^{286}Cn* decay via symmetric fission and the predicted fission mass region for GSkI and KDE0(v1) is 138 to 148, i.e., $A/2 \pm 5$. Further the quasifission peaks appears at ^{202}Pt (+ ^{84}Se), similar to one observed experimentally in superheavy nucleus $Z = 122$ [77]. This result is again independent of the choice of Skyrme force and is in complete agreement with experimental results [8,12]. The predicted fission cross section ($\sigma_{ff}^{\text{predicted}}$) for CN ^{286}Cn* at $E^* = 35$ MeV comes out to be 1.63×10^{-12} mb for GSkI force, 9.87×10^{-10} mb for KDE0(v1) force, and 3.38×10^{-17} mb for SIII force. In Table IV, we have also presented our calculations for the other proposed t-p combinations for "hot fusion" reactions at an illustrative $E^* = 34.4$ to 39.8 MeV, using the same neck length parameters as extracted from Fig. 11 and Table II for $^{238}\text{U} + ^{48}\text{Ca}$ reaction.

IV. SUMMARY AND CONCLUSIONS

Quantum mechanical fragmentation theory (QMFT), involving nuclear interaction potentials derived from SEDF

based on the semiclassical ETF approach with densities added in the frozen densities approximation, is used to identify the cold t-p combinations, referring to potential energy minima, for the formation of CN ^{286}Cn* at a fixed relative separation ΔR (within a nuclear limit of $\approx$2 fm) at a given excitation energy E^*. Both the conventional (SIII) and newer [GSkI and KDE0(v1)] Skyrme forces are used, which account for the properties of both the normal and isospin-rich nuclei, with nuclei considered quadrupole deformed and optimally hot oriented, lying in the same plane (coplanar nuclei). An interesting result is that, in addition to hot a fusion reaction, namely ^{238}U + ^{48}Ca already used in experiments to synthesize ^{286}Cn*, a number of other reactions are predicted which lie at minima in the PES, shown in Fig. 7 and Table I for Skyrme force KDE0(v1) along with their other characteristics: quadrupole deformations β_{2i}, calculated barrier heights V_B, and barrier positions R_B for optimum hot orientations. Of all the t-p combinations shown in Table I and Fig. 7, specifically ^{218}Po + ^{68}Ni and ^{202}Pt + ^{84}Se are suggested for synthesis of CN ^{286}Cn* in future experiments. We have also calculated channel cross sections for the predicted t-p combinations. These calculations are made for the hot-compact configuration since it favors symmetric fission, in complete agreement with experiments. The decay of ^{286}Cn* via 3n-4n emission is then studied by using the DCM with effects of quadrupole deformations and compact orientations. The Skyrme force included DCM is used to calculate the fusion excitation function of optimum hot fusion reactions ^{238}U + ^{48}Ca, giving a nice description of data, independently of Skyrme force used, within one-parameter fitting of neck length (ΔR). Further, we have also calculated experimentally unobserved 1n, 2n, and 4n evaporation cross sections at different $E^* = 34.4$ to 39.8 MeV by using the DCM model with the application of GSkI Skyrme force, and corresponding data are shown in Table III. The predicted fission mass region lies at A=138 to A=148, i.e., $A/2\pm5$, and the quasi-fission peaks appears at ^{202}Pt (+ ^{84}Se). The predicted fission cross section ($\sigma_{ff}^{\text{predicted}}$) for CN ^{286}Cn* at $E^* = 35$ MeV comes out to be 1.63×10^{-12} mb for GSkI force, 9.87×10^{-10} mb for KDE0(v1) force and 3.38×10^{-17} mb for SIII force.

ACKNOWLEDGMENTS

We are very grateful to late Emeritus Prof. Raj K. Gupta and Dr. Sahila Chopra (Women Scientist-A), Department of Physics, Panjab University, Chandigarh for their fruitful guidance and support for this work. One of the authors (Nirupama Kumari) would like to thank University Grants Commission (UGC) India for financial support under reference No. 1294/(CSIR-UGC NET JUNE 2017).

[1] Niyti *et al.*, J. Phys. G: Nucl. Part. Phys. **37**, 115103 (2010).
[2] Yu. Ts. Oganessian *et al.*, Eur. Phys. J. A **5**, 63 (1999).
[3] A. T. Kruppa, M. Bender, W. Nazarewicz, P.-G. Reinhard, T. Vertse, and S. Cwiok, Phys. Rev. C **61**, 034313 (2000).
[4] S. ćwiok, J. Dobaczewski, P. H. Heenen, P. Magierski, and W. Nazarewicz, Nucl. Phys. A **611**, 211 (1996).
[5] Yu. Ts. Oganessian, in *Proceedings of the International Conference Nuclear Physics at the Turn of the Millenium: "Structure of the Vacuum and Elementary Matter"*, Wilderness, South Africa (World Scientific, Singapore, 1996), p. 11.
[6] S. Hofmann, Rep. Prog. Phys. **61**, 639 (1998).
[7] Y. A. Lazarev, Y. V. Lobanov, Y. T. Oganessian, V. K. Utyonkov, F. S. Abdullin, A. N. Polyakov, J. Rigol, I. V. Shirokovsky, Y. S. Tsyganov, S. Iliev, V. G. Subbotin, A. M. Sukhov, G. V. Buklanov, B. N. Gikal, V. B. Kutner, A. N. Mezentsev, K. Subotic, J. F. Wild, R. W. Lougheed, and K. J. Moody, Phys. Rev. C **54**, 620 (1996).
[8] Y. T. Oganessian, V. K. Utyonkov, Y. V. Lobanov, F. S. Abdullin, A. N. Polyakov, I. V. Shirokovsky, Y. S. Tsyganov, G. G. Gulbekian, S. L. Bogomolov, B. N. Gikal, A. N. Mezentsev, S. Iliev, V. G. Subbotin, A. M. Sukhov, A. A. Voinov, G. V. Buklanov, K. Subotic, V. I. Zagrebaev, M. G. Itkis, J. B. Patin, K. J. Moody, J. F. Wild, M. A. Stoyer, N. J. Stoyer, D. A. Shaughnessy, J. M. Kenneally, P. A. Wilk, R. W. Lougheed, R. I. Ilkaev, and S. P. Vesnovskii, Phys. Rev. C **70**, 064609 (2004).
[9] R. K. Gupta, Niyti, M. Manhas, and W. Greiner, J. Phys. G: Nucl. Part. Phys. **36**, 115105 (2009).
[10] W. Loveland, K. E. Gregorich, J. B. Patin, D. Peterson, C. Rouki, P. M. Zielinski, and K. Aleklett, Phys. Rev. C **66**, 044617 (2002).
[11] K. E. Gregorich, W. Loveland, D. Peterson, P. M. Zielinski, S. L. Nelson, Y. H. Chung, Ch. E. Düllmann, C. M. Folden, K. Aleklett, R. Eichler, D. C. Hoffman, J. P. Omtvedt, G. K. Pang, J. M. Schwantes, S. Soverna, P. Sprunger, R. Sudowe, R. C. Wilson, and H. Nitsche, Phys. Rev. C **72**, 014605 (2005).
[12] S. Hofmann, D. Ackermann, S. Antalic, H. G. Burkhard, V. F. Comas, R. Dressler, Z. Gan, S. Heinz, J. A. Heredia, F. P. Hessberger, J. Khuyagbaatar, B. Kindler, I. Kojouharov, P. Kuusiniemi, M. Leino, B. Lommel, R. Mann, G. Münzenberg, K. Nishio, A. G. Popeko, S. Saro, H. J. Schött, B. Streicher, B. Sulignano, J. Uusitalo, M. Venhart, and A. V. Yeremin, Eur. Phys. J. A **32**, 251 (2007).
[13] K. J. Moody, in *Synthesis of Superheavy Elements*, 2nd ed., edited by M. Schädel and D. Shaughnessy (Springer-Verlag, Berlin, 2014), p. 26.
[14] J.-M. Mewes, O. R. Smits, G. Kresse, and P. Schwerdtfeger, Angew. Chem. Int. Ed. **58**, 17964 (2019).
[15] A. Heidari *et al.*, Adv. Sci. Eng. Med. **12**, 571 (2020).
[16] R. K. Gupta, in *Clusters in Nuclei*, edited by C. Beck, Lecture Notes in Physics No. 818, Vol. I (Springer-Verlag, Berlin, 2010), pp. 223–265.
[17] J. Sadhukhan, W. Nazarewicz, and N. Schunck, Phys. Rev. C **93**, 011304(R) (2016).
[18] H. Eslamizadeh, Phys. Rev. C **104**, 034601 (2021).
[19] B. Schuetrumpf and W. Nazarewicz, Phys. Rev. C **96**, 064608 (2017).
[20] T. Nakatsukasa, K. Matsuyanagi, M. Matsuo, and K. Yabana, Rev. Mod. Phys. **88**, 045004 (2016).
[21] A. S. Umar and V. E. Oberacker, Nucl. Phys. A **944**, 238 (2015).

[22] G. G. Adamian, N. V. Antonenko, W. Scheid, and V. V. Volkov, Nucl. Phys. A **633**, 409 (1998).
[23] G. Zhang, C. Li, P.-W. Wen, J.-J. Li, X.-X. Xu, B. Li, Z. Liu, and F.-S. Zhang, Phys. Rev. C **98**, 014613 (2018).
[24] B. Grammoticos and A. Voros, Ann. Phys. (NY) **123**, 359 (1979).
[25] M. Brack, C. Guet, and H.-B. Hakansson, Phys. Rep. **123**, 275 (1985).
[26] J. Bartel and K. Bencheikh, Eur. Phys. J. A **14**, 179 (2002).
[27] G.-Q. Li, J. Phys. G: Nucl. Part. Phys. **17**, 1127 (1991).
[28] R. K. Gupta, D. Singh, R. Kumar, and W. Greiner, J. Phys. G: Nucl. Part. Phys. **36**, 075104 (2009).
[29] R. K. Gupta, A. Sadulescu, and W. Greiner, Phys. Lett. **67B**, 257 (1977).
[30] J. Maruhn and W. Greiner, Phys. Rev. Lett. **32**, 548 (1974).
[31] R. K. Gupta, W. Scheid, and W. Greiner, Phys. Rev. Lett. **35**, 353 (1975).
[32] A. Sandulescu, R. K. Gupta, W. Scheid, and W. Greiner, Phys. Lett. **60 B**, 225 (1976).
[33] R. K. Gupta, Sov. J. Part. Nucl. **8**, 289 (1977).
[34] R. K. Gupta, M. Balasubramaniam, R. Kumar, D. Singh, C. Beck, and W. Greiner, Phys. Rev. C **71**, 014601 (2005).
[35] R. K. Gupta, M. Manhas, and W. Greiner, Phys. Rev. C **73**, 054307 (2006).
[36] A. Deep, Niyti, R. Kharab, R. Singh, and S. Chopra, Phys. Rev. C **102**, 034607 (2020).
[37] A. Deep, Niyti, R. Kharab, R. Singh, and S. Chopra, Int. J. Mod. Phys. E **28**, 1950079 (2019).
[38] R. K. Gupta, M. Balasubramaniam, C. Mazzocchi, M. La Commara, and W. Scheid, Phys. Rev. C **65**, 024601 (2002).
[39] R. K. Gupta, R. Kumar, N. K. Dhiman, M. Balasubramaniam, W. Scheid, and C. Beck, Phys. Rev. C **68**, 014610 (2003).
[40] M. Balasubramaniam, R. Kumar, R. K. Gupta, C. Beck, and W. Scheid, J. Phys. G: Nucl. Part. Phys. **29**, 2703 (2003).
[41] R. K. Gupta, M. Balasubramaniam, R. Kumar, N. Singh, M. Manhas, and W. Greiner, J. Phys. G: Nucl. Part. Phys. **31**, 631 (2005).
[42] R. K. Gupta, M. Balasubramaniam, R. Kumar, D. Singh, S. K. Arun, and W. Greiner, J. Phys. G: Nucl. Part. Phys. **32**, 345 (2006).
[43] R. K. Gupta, S. K. Arun, R. Kumar, and Niyti, Int. Rev. Phys. **2**, 369 (2008).
[44] B. B. Singh, M. K. Sharma, and R. K. Gupta, Phys. Rev. C **77**, 054613 (2008).
[45] S. K. Arun, R. Kumar, and R. K. Gupta, J. Phys. G: Nucl. Part. Phys. **36**, 085105 (2009).
[46] R. Kumar and R. K. Gupta, Phys. Rev. C **79**, 034602 (2009).
[47] R. Kumar, M. Bansal, S. K. Arun, and R. K. Gupta, Phys. Rev. C **80**, 034618 (2009).
[48] M. K. Sharma, G. Sawhney, R. K. Gupta, and W. Greiner, J. Phys. G: Nucl. Part. Phys. **38**, 105101 (2011).
[49] M. Kaur, R. Kumar, and M. K. Sharma, Phys. Rev. C **85**, 014609 (2012).
[50] M. K. Sharma, S. Kanwar, G. Sawhney, and R. K. Gupta, Phys. Rev. C **85**, 064602 (2012).
[51] M. Bansal, S. Chopra, R. K. Gupta, R. Kumar, and M. K. Sharma, Phys. Rev. C **86**, 034604 (2012).
[52] S. Chopra, M. Bansal, M. K. Sharma, and R. K. Gupta, Phys. Rev. C **88**, 014615 (2013).
[53] Niyti and R. K. Gupta, Phys. Rev. C **89**, 014603 (2014).
[54] Niyti, R. K. Gupta, and P. O. Hess, Nucl. Phys. A **938**, 22 (2015).
[55] H. Kröger and W. Scheid, J. Phys. G **6**, L85 (1980).
[56] R. K. Gupta, in *Nuclear Particle Correlations and Cluster Physics*, edited by W. U. Schröder (World Scientific Publishing, 2017), pp. 471–494.
[57] S. Kumar and R. K. Gupta, Phys. Rev. C **55**, 218 (1997).
[58] T. Matsuse, C. Beck, R. Nouicer, and D. Mahboub, Phys. Rev. C **55**, 1380 (1997).
[59] S. J. Sanders, D. G. Kovar, B. B. Back, C. Beck, D. J. Henderson, R. V. F. Janssens, T. F. Wang, and B. D. Wilkins, Phys. Rev. C **40**, 2091 (1989).
[60] S. J. Sanders, Phys. Rev. C **44**, 2676 (1991).
[61] N. J. Davidson, S. S. Hsiao, J. Markram, H. G. Miller, and Y. Tzeng, Nucl. Phys. A **570**, 61c (1994).
[62] G. Audi, A. H. Wapstra, and C. Thiboult, Nucl. Phys. A **729**, 337 (2003).
[63] W. Myers and W. J. Swiatecki, Nucl. Phys. **81**, 1 (1966).
[64] R. Kumar, M. K. Sharma, and R. K. Gupta, Nucl. Phys. A **42**, 870 (2011).
[65] Niyti, A. Deep, R. Kharab, S. Chopra, and R.K. Gupta, Phys. Rev. C **95**, 034602 (2017).
[66] B. K. Agrawal, S. K. Dhiman, and R. Kumar, Phys. Rev. C. **73**, 034319 (2006).
[67] D. Vautherin and D. M. Brink, Phys. Rev. C **5**, 626 (1972).
[68] B. K. Agrawal, S. Shlomo, and V. K. Au, Phys. Rev. C **72**, 014310 (2005).
[69] J. Blocki, J. Randrup, W. J. Swiatecki, and C. F. Tsang, Ann. Phys. (NY) **105**, 427 (1977).
[70] R. K. Gupta, N. Singh, and M. Manhas, Phys. Rev. C **70**, 034608 (2004).
[71] R. K. Gupta, D. Singh, and W. Greiner, Phys. Rev. C **75**, 024603 (2007).
[72] P. Chattopadhyay and R. K. Gupta, Phys. Rev. C **30**, 1191 (1984).
[73] L. R. B. Elton, *Nuclear Sizes* (Oxford University Press, London, 1961).
[74] H. de Vries, C. W. de Jager, and C. de Vries, At. Data Nucl. Data Tables **36**, 495 (1987).
[75] P. Möller, J. R. Nix, W. D. Myers, and W. J. Swiatecki, At. Nucl. Data Tables **59**, 185 (1995).
[76] Z.-H. Wu, L. Zhu, F. Li, X.-B. Yu, J. Su, and C.-C. Guo, Phys. Rev. C **97**, 064609 (2018).
[77] M. G. Itkis *et al.*, Nucl. Phys. A **734**, 136 (2004).